ORGANOMETALLICS

Article

pubs.acs.org/Organometallics

Electron Transfer and Modification of Oligosilanylsilatranes and Related Derivatives

Mohammad Aghazadeh Meshgi,[†] Judith Baumgartner,*[,‡] Viatcheslav V. Jouikov,*[,§] and Christoph Marschner*[,†]

[†]Institut für Anorganische Chemie, Technische Universität Graz, Stremayrgasse 9, 8010 Graz, Austria

[‡]Institut für Chemie, Universität Graz, Stremayrgasse 9, 8010 Graz, Austria

[§]UMR 6226, Chimie et Photonique Moléculaires, Université de Rennes 1, 35042 Rennes, France

Supporting Information

ABSTRACT: Several silatranyl -substituted oligosilanes were prepared starting from bis(trimethylsilyl)silatranylsilanide. Electrochemical and theoretical investigations of some oligosilanes revealed that electrooxidation occurs by formation of a short-lived cation radical. This species undergoes structural relaxation to form a pair of conformers, with endo and exo relationships with respect to the Si–N interaction. Reaction of a 1,4-disilatranyl-1,4-disilanide with 1,2-dichlorotetramethyldisilane gave a mixture of cis and trans diastereomers of a cyclohexasilane with the trans isomer showing a diminished Si–N distance.

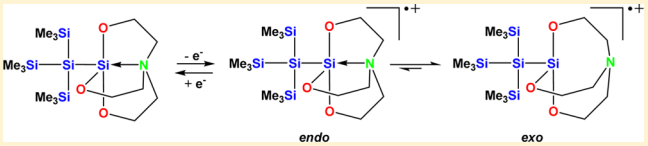

INTRODUCTION

Among hypercoordinated silicon compounds silatranes (Figure 1) occupy a prominent position.[1−4] The suffix "atrane" was originally proposed by Voronkov in 1966 for compounds where a central metalloid element such as silicon, boron, or aluminum is coordinated by a triethanolamine ligand, causing a transannular interaction of the donor nitrogen moiety and the acceptor element.[5]

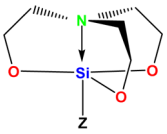

Figure 1. Silatrane structure.

With respect to a substituent Z occupying silicon's remaining valence there is a general relationship between the Si–Z and Si–N distances: longer Si–Z bond lengths (implying weaker Si–Z bonding interactions) usually result in shorter Si–N distances (suggesting stronger Si–N bonding interactions). This is consistent with the notion that the axial bonding in pentacoordinated compounds may be described in terms of three-center–four-electron (3c-4e) bonding.[6]

According to X-ray diffraction studies of silatranes with Z = H, halogen, aryl, alkyl, O, the Si–N distance ranges from 2.05 to 2.20 Å, which is significantly shorter than the sum of the van der Waals radii of silicon and nitrogen at 3.5 Å but is slightly longer than the typical covalent single Si–N bond distance of approximately 1.7–1.8 Å. In the gas phase the Si–N distance increases, suggesting a weaker Si–N interaction.[7] The high flexibility of the trigonal-bipyramidal structure of silatranes along the Si–N dative bond reflects the nature of Si–N bonding. In fact the Si–N bonding neither is covalent nor is based on intermolecular charge transfer.[8] What happens with this unusual bond upon electron withdrawal, for instance during electrooxidation, is of a great interest (for classical bonds see ref 9) but is not known so far. Only scarce reports exist on the oxidation of 1-organosilatranes,[10−12] though preliminary data on the cation radicals of organogermatranes[13] suggest it might be very insightful.

Interestingly, a survey of known sila- and germatranes with different triethanolamine substituents reveals that, despite the large variety of attached groups Z which have been studied, almost no compounds of atranes with bonds to other heavy group 14 elements exist.[14] After the first studies by Zaitsev et al., addressing germylated germatranes,[15] and Yamamoto et al., studying the potential of silylated silatranes as silyltransfer regents,[16] we have disclosed our initial studies on oligosilylated silatranes including some derivatization chemistry.[17] In the current account we wish to extend this.

RESULTS AND DISCUSSION

Synthesis. In the view of our recent effort concerning the investigation of conformational properties of oligosilanes,[18−23] we were interested in studying the effects of silatranyl groups on the electronic properties of oligosilanes. For this reason we prepared tris(trimethylsilyl)silylsilatrane (**1**) by reaction of tris(trimethylsilyl)silylpotassium[24] with silatranyl triflate (Scheme 1).[17] An analogous reaction of silatranyl triflate was done with tris(trimethylsilyl)germylpotassium,[25] and the

Received: October 13, 2016
Published: December 20, 2016

DOI: 10.1021/acs.organomet.6b00786
Organometallics 2017, 36, 342−351

Scheme 1. Formation of Oligosilanylsilatranes using Salt Elimination Reactions

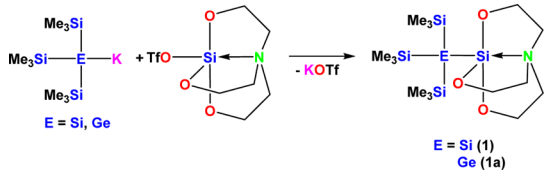

respective tris(trimethylsilyl)germylsilatrane (**1a**) was obtained. The related tris(trimethylsilyl)germylgermatrane was obtained previously by Zaitsev et al. using germatranyl triflate.[15] The NMR spectroscopic properties of **1a** are very similar to those of **1**. The ^{1}H and ^{13}C signatures of the silatrane cage are almost identical (Table 1). In the ^{29}Si NMR spectrum the silatranyl signal at −53.3 ppm is clearly indicating that there is a hypercoordinative interaction between the nitrogen and the SiO_3 unit.[1−4] The analogous signal of $(Me_3Si)_3SiSi(OMe)_3$,[26,27] where the silicon atom has the same substitution pattern but no hypercoordinative interaction, can be found at −32.2 ppm.

The only significant differences in the ^{29}Si spectra of **1** and **1a** are the missing quaternary silicon atom for **1a** and the signal for the Me_3Si groups located at −5.6 ppm, which is a perfectly reasonable chemical shift for $(Me_3Si)_3Ge$ groups.[24]

The solid-state structure of **1a** (Figure 2) in the crystal is also similar to that of **1**. Cell parameters of both compounds crystallizing in the triclinic space group $P\bar{1}$ are rather similar. The Si···N distance of 2.250(9) Å for **1a** is a bit shorter than the 2.292(3) Å found for **1**, which indicates that the $(Me_3Si)_3Ge$ unit is less electron donating than $(Me_3Si)_3Si$ (Table 2).

As our previous studies on oligosilanes and germanes have relied on the facile trimethylsilyl group abstraction using KO^{t}Bu, we were pleased to find that compounds **1** and **1a** smoothly undergo reactions with KO^{t}Bu in the presence of 18-crown-6 to form the respective silanide **2**[17] and germanide **2a** (Scheme 2). Again **2** and **2a** are very similar with respect to their spectroscopic properties. The ^{1}H and ^{13}C spectra are almost identical (Table 1), and for the case of the ^{29}Si spectra only the missing silanide resonance at −210.5 ppm distinguishes **2** from **2a** (Table 1). The SiO_3 resonance at −13.0 ppm, which is a typical value for a tetracoordinate silicon atom with this particular substitution pattern, clearly shows that no Si···N interaction is any longer present. Confirmation for this is provided by the crystal structure of **2a** (Figure 3), which exhibits a long Si−N distance of 3.131(5) Å (Table 2). Again

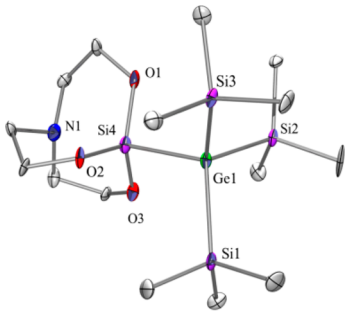

Figure 2. Molecular structure of **1a** (thermal ellipsoid plot drawn at the 30% probability level). All hydrogen atoms are omitted for clarity. Bond lengths (Å) and angles (deg): Si(1)−C(1) 1.87(2), Si(1)−Ge(1) 2.379(5), Si(2)−Ge(1) 2.358(5), Si(3)−Ge(1) 2.367(5), Si(4)−Ge(1) 2.378(3), O(1)−C(10) 1.42(2), O(1)−Si(4) 1.674(13), C(10)−C(11) 1.49(3), C(11)−N(1) 1.54(2), Si(4)−N(1) 2.250(10); Si(2)−Ge(1)−Si(11) 81.0(3), Si(2)−Ge(1)−Si(3) 109.99(18), O(3)−Si(4)−O(2) 117.3(7), O(1)−Si(4)−O(2) 117.1(7), N(1)−Si(4)−Ge(1) 179.2(3).

the structures of **2** and **2a** are very similar, both crystallizing in the monoclinic space group $P2_1/n$ with nearly identical cell parameters.[17]

For an understanding of the influence of a silatranyl substituent on the σ-electron delocalization of oligosilanes, compound **1** is of limited use, as UV spectroscopic studies of the delocalization phenomenon typically require chains of at least five or six linearly connected silicon atoms.[22] Therefore, we used silatranylsilanide **2** to prepare the hexasilanes **3**[17] and **4**[17] by reacting it with the appropriate chlorosilanes Cl-$(SiMe_2)_2$Cl and Cl$(SiMe_2)_2Si(SiMe_3)_3$ (Scheme 2).[17]

The UV spectra of compounds **3** and **4** were compared to those of the structurally related compounds 2,2,5,5-tetrakis-(trimethylsilyl)decamethylhexasilane (**5**)[28] and 2,5-bis-(trimethylsilyl)dodecamethylhexasilane (**6**),[29] which also contain hexasilane units as the longest chain segments. Comparison of the low-energy bands associated with the longest chain segments revealed that for compound **3**, containing one silatranyl group, the longest wavelength absorption band (254 nm) shows a 2 nm hypsochromic shift with respect to **5**.[17]

The same band is shifted further toward blue by another 2 nm for compound **4**. While the molecular structure of **4** in the solid state indicates the silatranyl units to be part of the all-transoid hexasilane conformer, it needs to be pointed out that for **3** and **4** in solution rotational processes of the bulky tris(trimethylsilyl)silyl and bis(trimethylsilyl)silatranylsilyl

Table 1. NMR Spectroscopic Data of Oligosilanyl and Silylgermyl Silatranes and Related Compounds

	^{29}Si					
	$SiMe_3$	SiO_3	Si_q	other	^{13}C (OCH_2/CH_2N)	^{1}H (OCH_2/CH_2N)
1[a,b]	−9.9	−52.6	−133.9		58.6/52.2[b]	3.65/2.72[b]
					58.6/51.5[c]	3.30/1.83[c]
1a[b]	−5.6	−53.2	na		58.6/52.2	3.67/2.73
$(Me_3Si)_3SiSi(OMe)_3$[c,d]	−9.8	−32.2	−141.1		na	na
2[c]	−3.2	−11.8	−210.5		61.0/54.3	3.86/2.84
2a[c]	−2.0	−13.0	na		60.9/54.2	3.84/2.83
7[c]	−2.3	−9.9	−209.0	−24.1 (Me_2Si)	61.0/54.5	3.92/2.91
***cis*-8**[c]	−7.8	−50.7	−129.9	−37.5 (Me_2Si)	59.0/51.9	3.40/1.92
***trans*-8**[c]	−6.4	−52.3	−130.3	−36.2 (Me_2Si)	58.9/51.7	3.37/1.90

[a]Data taken from ref 17. [b]Measured in $CDCl_3$. [c]Measured in C_6D_6. [d]Data taken from refs 26 and 27.

DOI: 10.1021/acs.organomet.6b00786
Organometallics 2017, 36, 342−351

Table 2. Compilation of Structural Data Derived by Single-Crystal XRD Analysis of 1a, 2a, *cis*-8, and *trans*-8

	d(Si···N) (Å)	d(E−SiO$_3$) (Å)	d(E−SiMe$_3$) (Å)	∠Me$_3$SiESi (deg)	∑∠SiSiR (deg)
1	2.292(3)	2.351(2)	2.335(2)−2.341(2)		
1a	2.250(10)	2.378(3)	2.367(6), 2.358(5), 2.380(6)	110.0(2), 109.8(2), 110.3(2)	330.1(2)
2	3.134(4)	2.308(2)	2.312(2)/2.318(2)		
2a	3.131(5)	2.355(2)	2.355(2), 2.359(2)	101.95(6)	359.40(5)
***cis*-8**	2.2912(15)/2.3326(15)	2.3447(8)/2.3429(7)	2.3427(8), 2.3455(8)		331.41(2), 336.31(2)
***trans*-8**	2.194(2)	2.3639(10)	2.339(1)		327.18(3)

Scheme 2. Derivatization of Oligosilanylsilatranes

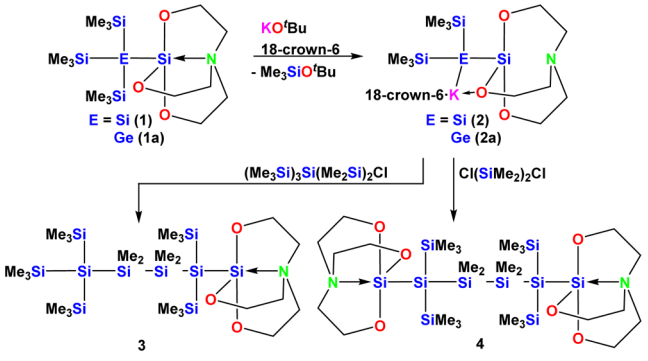

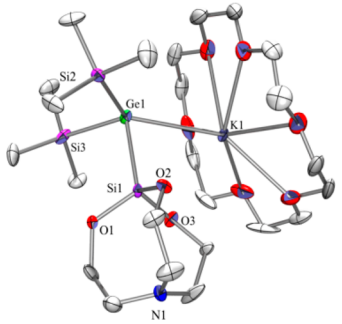

Figure 3. Molecular structure of **2a** (thermal ellipsoid plot drawn at the 30% probability level). All hydrogen atoms are omitted for clarity. Bond lengths (Å) and angles (deg): O(1)−C(1) 1.475(10), O(1)−Si(1) 1.633(5), C(1)−C(2) 1.492(11), Ge(1)−Si(1) 2.3552(16), Ge(1)−Si(3) 2.3554(19), Ge(1)−Si(2) 2.3588(16), Ge(1)−K(1) 3.3393(14), N(1)−C(2) 1.444(10), Si(2)−C(7) 1.875(7); Si(1)−Ge(1)−Si(3) 96.29(6), Si(1)−Ge(1)−Si(2) 97.87(6), Si(3)−Ge(1)−Si(2) 101.94(6), Si(1)−Ge(1)−K(1) 81.98(4), Si(3)−Ge(1)−K(1) 126.17(5), Si(2)−Ge(1)−K(1) 131.73(5), O(1)−Si(1)−O(3) 109.2(3), N(1)−C(6)−C(5) 119.8(7).

groups are likely to be facile and therefore all-transoid hexasilane conformers with trimethylsilyl end groups are presumably contributing to the hexasilane absorption band. Conversely, for 2,5-bis(trimethylsilyl)dodecamethylhexasilane (**6**), where two trimethylsilyl groups are exchanged for methyl groups, the hexasilane band shows a bathochromic shift of 7 nm to an absorption maximum of 263 nm.[17] This behavior is consistent with the typically observed trend of electron-withdrawing substituents causing a bathochromic shift of the absorption maxima and electron-donating groups being responsible for a contrary behavior.[30]

Voltammetry. In order to gain further insight into the electronic structures of **3** and **4**, electrochemical measurements were conducted. Oxidation of these oligosilanyl silatranes was carried out in CH$_3$CN/0.1 M Bu$_4$NPF$_6$ at Pt and glassy-carbon (GC) disk electrodes. Although solubility does not allow obtaining solutions more concentrated than 2−3 mmol L^{-1} in this media, both compounds exhibit reasonably well shaped oxidation peaks in the range 1.3−1.5 V vs SCE. On the reduction side, **3** and **4** do not show any cathodic reduction up to −3.1 V, which is in line with the fact that neither polysilane chains[31,32] nor the silatranyl moiety (a strong electron donor itself)[33] are reducible electrochemically.

The first oxidation potentials of **3** and **4** (E_p = 1.332 and 1.335 V, respectively) are practically similar, showing that there is no noticeable electronic interaction between the two silatrane units in **4**. Their oxidation peaks are diffusion-controlled ($i_p/v^{1/2}$ is invariable with the scan rate for v = 0.1−10 V s^{-1}), which allows determining the number of electrons transferred at the first step using the diffusion-controlled one-electron oxidation current of ferrocene under similar conditions or else combining $i_p v^{-1/2}$ with the Cottrell slope $it^{1/2}$ from chronoamperometry.[34] Both methods converge at the electron stoichiometry n = 1. With this, the half-widths of the first oxidation peaks ($E_{p\text{-}p/2}$ = 160 mV for **3** and 147 mV for **4**) are much larger than that for an electrochemically reversible process ($\Delta E_{p\text{-}p/2}$ = 57 mV). The reverse peaks (reduction of the species issued from the oxidation at E_p^a) observed for these silatranes at reasonably high scan rates (Figure 4) are also shifted to less positive

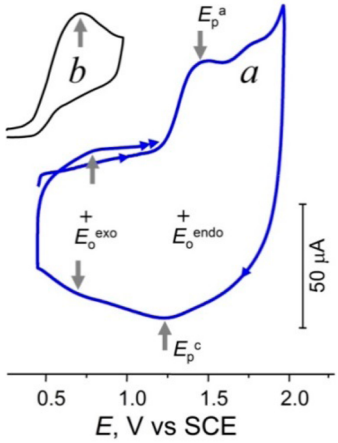

Figure 4. (a) Cyclic voltammogram of the oxidation of **3** (2.2 mmol L^{-1}) in CH$_3$CN/0.1 M Bu$_4$NPF$_6$ at a GC disk electrode. Conditions: T = 20 °C, v = 0.2 V s^{-1}. (b) Irreversible oxidation of N(CH$_2$CH$_2$OH)$_3$ under similar conditions.

potentials with E_p^a−E_p^c peak separations of 80−85 mV at 20 °C. These facts characterize the primary oxidation steps of **3** and **4** as quasi-reversible (apparent E_0^{endo}), resulting in the corresponding cation radicals whose relaxation to the stable geometry requires substantial reorganization energy.

For **4**, the first oxidation peak is followed by a second oxidation (E_p^2 = 1.62 V), which has a similar electron stoichiometry of n = 1 and is apparently electrochemically (quasi-)reversible; this step was assigned to the oxidation of the

DOI: 10.1021/acs.organomet.6b00786
Organometallics 2017, 36, 342−351

second silatranyl unit occurring at slightly more positive potentials because of the positive charge carried by the oxidized first silatranyl group. Increasing the scan rate reveals that the electron transfer (ET) kinetics of the first step starts limiting the overall rate of oxidation at $\nu > 2-5$ V s^{-1} and the peak width $\Delta E_{p\text{-}p/2}$ increases above 300 mV with no substantial increase in the cathodic counterpart of the main anodic peak.

At more positive potentials, silatrane **3**—like other known silatranes—shows a small peak ($E_p \cong 1.8$ V) supposedly arising from further oxidation of its cation radical to the dication. It is noteworthy that on the reverse scan in square-wave cyclic voltammetry (SWCV) one can notice a weak signal corresponding to the reduction of the $\mathbf{3}^{2+}$ back to $\mathbf{3}^{\bullet+}$ (Figure 5). For **4**, two one-electron consecutive oxidations of two

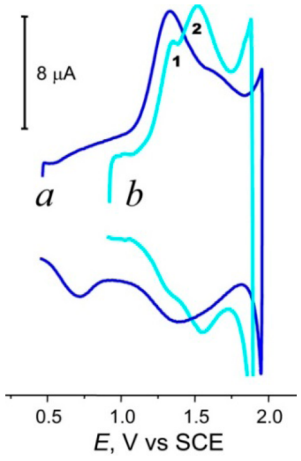

Figure 5. SWCV curves of the oxidation of (a) **3** and (b) **4** (both at 2.2 mmol L^{-1}) in CH_3CN/0.1 M Bu_4NPF_6 at a GC disk electrode. Conditions: T = 20 °C, ν = 0.333 V s^{-1}. Two reversible one-electron oxidations of both silatranyl units are seen for **4**.

silatranyl units (peaks 1 and 2) take place before the potential of formation of the dication, which is now shifted to ca. 2 V. The SWCV of **4** shows both oxidation steps to have cathodic counterparts. Interestingly, an additional reduction signal appears on the reverse scan in CV of **3** (Figure 4), corresponding to a new redox couple with less anodic standard potential (E_0^{exo} = 0.67 V), quite close to but slightly higher than E_p of the irreversible oxidation of $N(CH_2CH_2OH)_3$. The reduction component of this new redox couple is well seen in SWCV (Figure 5). Since the nitrogen lone pair in the exo form (with stretched N–Si distance) is supposed to be much less involved in a 3c-4e interaction and hence be better available for ET, this redox pair was assigned to the exo form $\mathbf{3}^{\bullet+}/\mathbf{3}$ (E_0^{exo}).

DFT Modeling. The oxidation of di- and polysilane derivatives usually requires potentials of 1.3–1.7 V vs SCE,[31,32,35–41] which are overlapping with the range of the few known oxidation E_p values of silatranes, 1.4–1.8 V.[10–12] Since the silatranyl moiety is a good electron donor[2,33] and is able to ease the oxidation of the connected redox units,[42] it might create a confusion as to the place of electron withdrawal from **3** and **4**. In this respect, germanium analogues of silatranes were earlier classified into two groups, according to their oxidation pattern which depends on the substituent at Ge—"proper" germatranes, i.e. those where the oxidation affects the atrane cage, and the others, with a substituent whose own oxidation potential is lower than that of the atrane unit.[13]

A similar principle is expected to apply to the silatrane family. In order to reveal the reaction site of oxidation in **3** and **4**, DFT calculations on the model compound [(trimethylsilyl)silyl]-silatrane—both on its neutral form (**1**) and on its cation radical ($\mathbf{1}^{\bullet+}$)—were carried out at the B3LYP/Lanl2DZ level under vacuum and in acetonitrile (AN) solution (accounted for through the CPCM model with ε = 36). Along with the main geometrical parameters, the N–Si distance (2.3 Å in AN vs 2.29 Å from X-ray diffractometry)[17] was very well reproduced by the calculations. Both calculations localize the HOMO on the silatrane unit, with the dominant contribution from the N lone pair and the 3e-4c character of HOMO being well-defined in both cases; the separation of HOMO from HOMO-1 and HOMO-2 being similar in AN (Figure 6). The next lower lying orbitals, HOMO-1 and HOMO-2 (the combinations of Si–Si σ-bonds of the oligosilyl substituent orthogonal to the 3c-4e system), are 0.13 and 0.18 eV (vacuum) and 0.02 eV (AN) lower in energy; therefore, the electron withdrawal upon oxidation most probably affects the N-based 3c-4e silatrane system of this compound, as in other "proper" silatranes.[11,12]

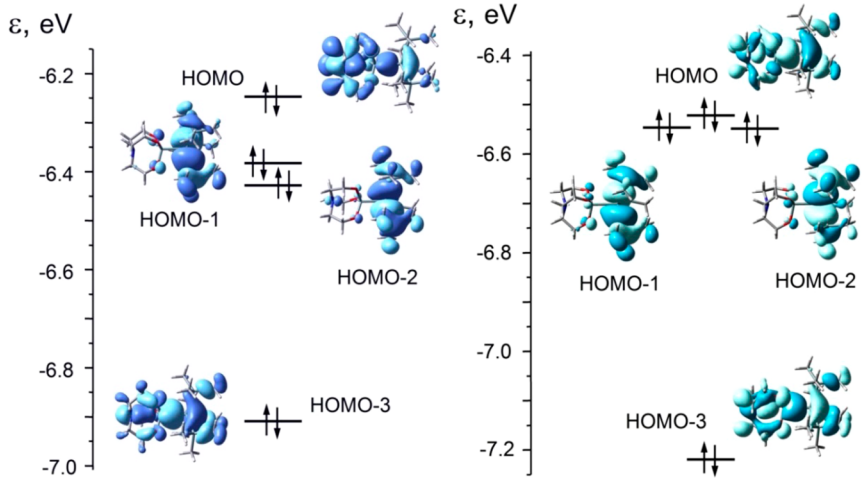

Figure 6. Atrane cage-located HOMO of $(Me_3Si)_3Si–Si(OCH_2CH_2)_3N$ (**1**) and lower-lying filled orbitals under vacuum (left) and in acetonitrile (right) from DFT B3LYP/Lanl2DZ calculations. The N lone pair electrons and the Si–Si σ-bond components of the 3c-4e system are clearly seen in the HOMO.

DOI: 10.1021/acs.organomet.6b00786
Organometallics 2017, 36, 342–351

Note that though the energy difference in the solution is very small (ca. 0.5 kcal mol^{-1}), the orthogonality of HOMO and HOMO-1,2 preserves them from hybrid formation so that they remain individual orbitals. Thus, though *irreversible* oxidation of the related oligosilane $(Me_3Si)_4Si$—the substituent-forming unit in **1**, **3**, and **4**—occurs at E_p = 1.43 V vs SCE, i.e. very close to E_p(**3**) and E_p(**4**), the *reversible* ET from the atrane cage in these compounds seems more probable than the oxidation of the substituent. The DFT calculations agree well with the experimental observation of only one oxidation step for **3** and of two steps for **4** corresponding to the electron withdrawal from one or two silatranyl units, respectively (Figures 4 and 5), and with quasi-reversible character of their oxidation. Note that the oxidation of linear and cyclic polysilanes is usually electrochemically irreversible and involves Si−Si bond cleavage.[35,38,39]

In neutral silatranes, the length of the N→Si intramolecular bond is very sensitive to the polarity of the substituents at Si[2,3] so that the positive charge induced by one-electron withdrawal is expected to provoke even stronger changes in the atrane cage geometry. The potential energy (PE) profiles of **1** and **1**$^{+\bullet}$ at different N−Si distances were therefore calculated at the B3LYP/Lanl2DZ level. The neutral silatrane has a sole energy minimum corresponding to its endo configuration (Figure 7).

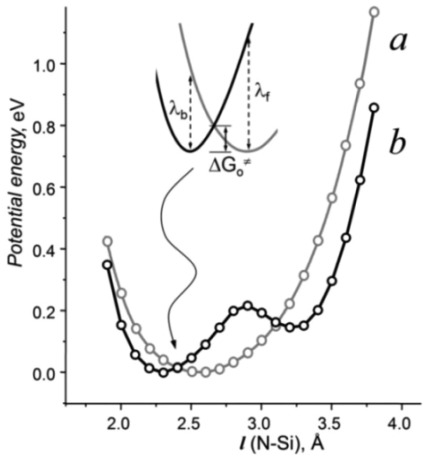

Figure 7. Gas-phase PE profiles of neutral **1** (a) and of its cation radical (b), plotted at zero driving force (from DFT B3LYP/Lanl2DZ). The inset shows λ_f and λ_b, the forward and backward reorganization energies, and the standard activation barrier $\Delta G_0^{\ddagger}$ for the **1**$^{+\bullet}_{endo}$/**1** redox pair.

In contrast and very interestingly, **1**$^{+\bullet}$ exhibits two stable geometries, endo and exo. Under vacuum, the endo form (with an N−Si distance 0.25 Å shorter than that in **1**) is preferred over the exo form (0.65 Å longer N−Si distance), which is in contrast with the data of voltammetry suggesting, on the basis of the i_p values assigned to the corresponding forms, the inverse order, in favor of the exo form. In solution, the situation is reversed and agrees with the experiment: **1**$^{+\bullet}_{exo}$ is now at −0.134 eV ($K_{exo/endo}$ = 1.8 × 10^2), an energetically favored global minimum. The value of $K_{exo/endo}$ supports the quite high reorganization requirement responsible for the quasi-reversible character of electron withdrawal and the observed absence of an increase in i_c/i_a ratio with scan rate. This is in line with the narrower (smaller E_p−$E_{p/2}$) reduction peak of **1**$^{+\bullet}_{exo}$ in comparison to the endo form. The difference in orbital energies ε_{SOMO} of the two cation radicals is 0.34 eV (7.85 kcal mol^{-1}) in favor of **1**$^{+\bullet}_{exo}$, which is also in good agreement with the difference of $E_0^{exo/endo}$ from CV.

In AN, structural differentiation of both forms from neutral **1** is more distinct: the N−Si distance in **1**$^{+\bullet}_{endo}$ and **1**$^{+\bullet}_{exo}$ is respectively 0.4 Å shorter and 0.8 Å longer than that in **1**. The practically parabolic PE profile of **1**$^{+\bullet}_{exo}$ (Figure 8) is separated

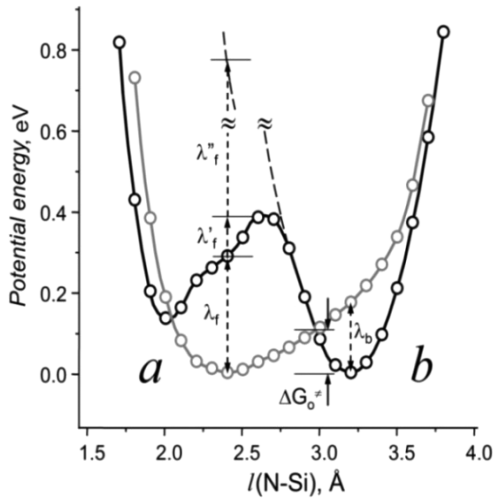

Figure 8. PE profiles of neutral **1** (a) and of the cation radical **1**$^{+\bullet}$ (b) in AN solution at zero driving force (from DFT B3LYP/Lanl2DZ CPCM calculations). The corresponding entities λ_f, λ_b, and $\Delta G_0^{\ddagger}$ are as in Figure 7.

from the endo form by an interconversion barrier of 0.38 eV (≅10 kcal mol^{-1}; i.e. 4 times that under vacuum). Both experiment and calculations in AN are thus in agreement with the character of hypercoordination at Si[2], implying that a longer N−Si distance (and a shorter (N→)Si−Si(1) length) should be observed in case of the atrane-localized oxidation (weakening N→Si interaction), while oxidation on the oligosilanyl substituent would shorten this distance, similarly to the effect of acceptor substituents at Si.[2,3]

The PE profile of the cation radical not being symmetrical, the minimum of **1** falls between those of the two forms of **1**$^{+\bullet}$. In this case, applying a Marcus ET treatment on the basis of the harmonic oscillator model[43] is somewhat tricky because of a complex nonparabolic pattern of the PE curve between the two minima: first, the standard activation energy $\Delta G_0^{\ddagger}$ no longer equals $\lambda/4$; its values can therefore be directly taken from the calculated PE for **1** and **1**$^{+\bullet}$ (Figure 8; note that a small $\Delta G_0^{\ddagger}$ value is consistent with the reversible character of ET).

Second, the reorganization energy λ_f from the ground state of **1** to the crossing with the PE profile of the cation radical is 0.287 eV; an additional 0.096 eV (λ_f') is required to reach the transition state between the endo and exo forms of **1**$^{+\bullet}$. This totals 0.383 eV needed for accomplishing the transition **1** → **1**$^{+\bullet}_{exo}$ on the reaction coordinate. A classical parabolic approach (Figure 8, dotted line) would imply a much higher reorganization energy, $\lambda_f + \lambda_f' + \lambda_f'' \cong 1.44$ eV, which seems improbable. Adiabatic ionization potentials (ΔG_0) related to **1**$^{+\bullet}_{exo}$ and **1**$^{+\bullet}_{endo}$ and the reorganization (λ_f) and activation ($\Delta G_0^{\ddagger}$) parameters from DFT calculations[44] allow assessing the relative rates of ET within these redox pairs by simply combining two quadratic activation-driving force equations:[43,45]

DOI: 10.1021/acs.organomet.6b00786
Organometallics 2017, 36, 342−351

$$\Delta G^{\ddagger}_{endo} = \Delta G^{\ddagger}_{0,endo}\left(1 - \frac{\Delta G^{0}_{endo}}{\lambda_f^{endo}}\right)^2$$

$$\Delta G^{\ddagger}_{exo} = \Delta G^{\ddagger}_{0,exo}\left(1 - \frac{\Delta G^{0}_{exo}}{\lambda_f^{exo}}\right)^2$$

Then, supposing the practical equality of the pre-exponential factors Z for both cation radicals, the ET rate constants can be related from $\exp(\Delta G^{\ddagger}_{endo} - \Delta G^{\ddagger}_{exo})$ as $k_s^{endo} \cong 9.48 k_s^{exo}$.

The situation can be rationalized (Scheme 3) as the formation of an endo cation radical (implied by the least motion principle)[46] with its following conversion to the thermodynamic product $\mathbf{1}^{\bullet+}_{exo}$. In fact, ET to form $\mathbf{1}^{\bullet+}_{endo}$ is faster (from $\Delta G^{\ddagger}$), but the formation of $\mathbf{1}^{\bullet+}_{exo}$ is preferable because its activation barrier is lower than the total gain in energy (ΔG_0). However, practical invariance of the reduction peaks of the two forms (i_p^{endo}/i_p^{exo}) with the scan rate suggests that they are not related by an ECE-type sequence[47] but rather belong to a common Curtin–Hammett kinetic scheme[46] realized in the electrochemical context.

Scheme 3. Redox Transformations at the Oxidation of 1

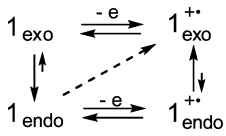

Derivatization. The fact that compounds **1** and **1a** can easily be converted into **2** and **2a** (Scheme 2) is highly encouraging, as it allows the facile use of the respective anions as building blocks.[17] Further extending this chemistry, we were interested in reacting compound **4** with 2 equiv of KO^{t}Bu (Scheme 4). Similar to an analogous reaction of **5**,[29,48] it was possible to obtain the 1,4-disilanide **7** in the presence of 2 equiv of 18-crown-6 (Scheme 4). The NMR spectroscopic properties of **7** are very similar to those of **2** (Table 1). Again in the ^{29}Si spectrum the SiO_3 resonance at −9.9 ppm clearly indicates no Si–N interaction. The $SiMe_3$ resonances at −2.3 ppm are typical for trimethylsilyl groups attached to a silanide. The most interesting peak in the ^{29}Si spectrum is that at −209.0 ppm (Table 1), which shows the typical upfield shift for silylated silanides. While such resonances are usually found around −190 ppm, the further upfield shift results from coordination of the potassium ion to a silatrane oxygen atom. This causes a higher degree of ion pair separation, which is reflected by the chemical shift.

Further reaction of **7** with 1,2-dichlorotetramethyldisilane proceeded to the expected cyclohexasilane **8**, which formed as a mixture of the cis and trans diastereomers (Scheme 4). Compounds ***cis*-8** and ***trans*-8** could be separated by crystallization from different solvent mixtures. Single-crystal X-ray diffraction studies of both diastereomers showed that the six-membered ring in the cis isomer (Figure 9) resembles the previously reported 1,1,4,4-tetrakis(trimethylsilyl)-octamethylcyclohexasilane,[49] which exhibits a twisted-boat conformation.[50] In contrast to this, ***trans*-8** (Figure 10) was found to engage in the typical chair conformation, with the silatranyl units occupying the axial positions. In cases of cyclohexanes typically the sterically more demanding substituents prefer the equatorial positions. This seems to indicate that the local steric demand of the silatranyl units is smaller

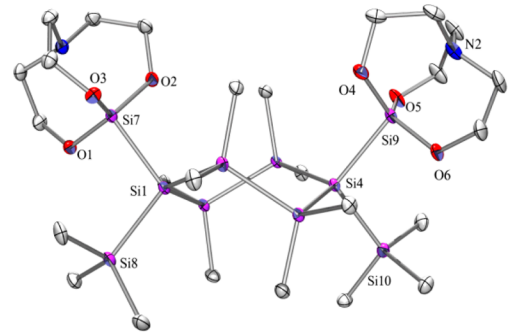

Figure 9. Molecular structure of ***cis*-8** (thermal ellipsoid plot drawn at the 30% probability level). All hydrogen atoms are omitted for clarity. Bond lengths (Å) and angles (deg): Si(1)–Si(7) 2.3447(8), Si(1)–Si(8) 2.3454(7), Si(1)–Si(6) 2.3527(8), Si(1)–Si(2) 2.3540(7), Si(2)–C(1) 1.8966(17), Si(4)–Si(9) 2.3429(7), Si(7)–O(1) 1.6676(12), Si(7)–N(1) 2.2912(15), Si(9)–O(4) 1.6572(12), Si(9)–N(2) 2.3326(15), N(1)–C(16) 1.460(2), N(2)–C(21) 1.462(3), O(1)–C(15) 1.418(2), O(4)–C(23) 1.421(2), C(17)–C(18) 1.512(2); Si(7)–Si(1)–Si(8) 104.75(2), Si(5)–Si(4)–Si(9) 109.97(2), O(2)–Si(7)–O(1) 117.62(6), O(4)–Si(9)–O(5) 115.53(7), O(4)–Si(9)–O(6) 116.64(7), C(16)–N(1)–C(18) 114.20(13).

Scheme 4. Conversion of the 1,4-Disilatranyloligosilane 4 to the Respective 1,4-Disilanide 7 and Further to the 1,4-Disilatranylcyclohexasilane 8, Which Forms as a Mixture of Two Diastereomers

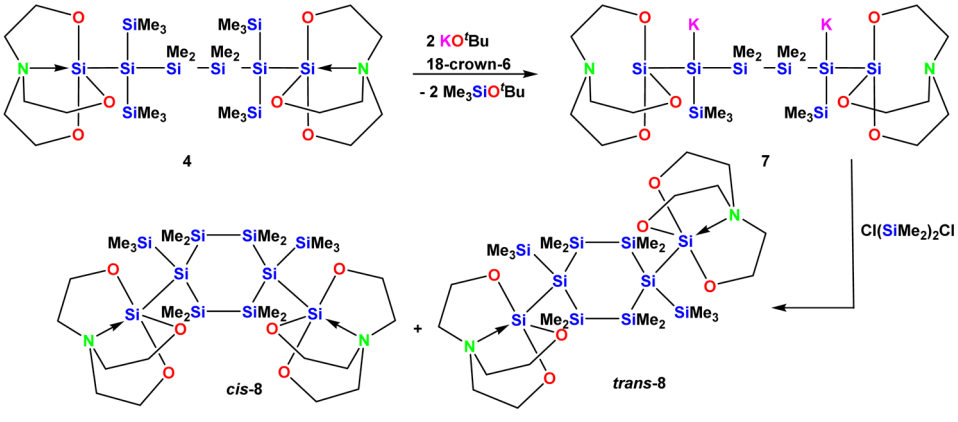

DOI: 10.1021/acs.organomet.6b00786
Organometallics 2017, 36, 342–351

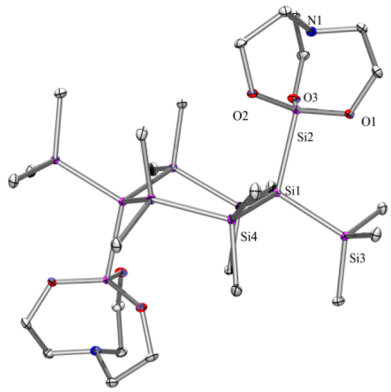

Figure 10. Molecular structure of ***trans*-8** (thermal ellipsoid plot drawn at the 30% probability level). All hydrogen atoms are omitted for clarity. Bond lengths (Å) and angles (deg): Si(1)−Si(2) 2.3639(10), Si(4)−C(10) 1.890(3), Si(2)−O(1) 1.6731(18), Si(2)−N(1) 2.194(2), O(1)−C(1) 1.421(3), N(1)−C(2) 1.470(3), C(2)−C(1) 1.522(4); Si(3)−Si(1)−Si(4) 107.57(4), Si(3)−Si(1)−Si(5) 110.31(4), Si(4)−Si(1)−Si(5) 109.32(4), Si(3)−Si(1)−Si(2) 107.23(3), Si(4)−Si(1)−Si(2) 110.58(3), Si(5)−Si(1)−Si(2) 111.74(4), C(4)−N(1)−C(2) 114.5(2).

than that of the trimethylsilyl groups. Given that Si−O bonds are shorter than Si−C bonds, this makes some sense. However, the oxygen atoms around the silatrane silicon atom are located in pseudoequatorial positions, bringing them in closer proximity to the tetrasilylated silicon atom in comparison to the methyl carbon atoms of the trimethylsilyl groups. This seems to suggest that the silatrane preference for axial positions is not only caused by steric reasons. It is likely that the orientation of the rather polar Si−Si−N units in the crystal plays a role. The NMR spectroscopic properties of ***cis*-8** and ***trans*-8** (Table 1) are very similar. The SiO_3 resonance of ***cis*-8** (−50.7 ppm) is slightly less shielded than that of ***trans*-8** (−52.3 ppm), indicating less Si−N interaction. This assumption is supported by the XRD data of ***cis*-8** and ***trans*-8** (Table 2), which show profoundly different Si−N distances of 2.2912(15)/2.3326(15) Å for ***cis*-8** and 2.194(2) Å for ***trans*-8**. It seems likely that the very short Si−N distance for ***trans*-8** is in part caused by the crystal packing and the trans geometry seems also to facilitate this interaction by a compensation of dipole moment.

It is known that alkylated cyclosilanes ($(R_2Si)_n$, n = 3−7) with smaller ring size exhibit a hypsochromic shift in the UV absorption spectrum, while on a further increase in the ring size the absorption behavior resembles more the linear compounds with bathochromic shifts.[51] The UV absorption spectrum of 1,1,4,4-tetrakis(trimethylsilyl)octamethylcyclohexasilane shows two bands at 246 and 268 nm,[22] whereas the related spectrum of ***cis*-8** exhibits a band at 242 nm and a trailing shoulder around 270 nm. The spectrum of ***trans*-8** finally does not show distinct bands. A shoulder that is not well resolved appears slightly blue shifted in comparison to ***cis*-8**. This picture is consistent with the hypsochromic shift of **4** in comparison to **5** that is described above.

CONCLUSION

The recent report of the tris(trimethylsilyl)silylated silatrane **1** and its conversion to the related potassium silanide **2**[17] have added the silatranyl substituent to the toolbox of oligosilane chemistry. Its influence on σ-bond electron delocalization was analyzed by UV spectroscopy using the related oligosilanes **3** and **4**. In order to gain a better insight into silatranyl-substituted oligosilanes, electrochemical studies were carried out, accompanied by a theoretical study using DFT methods. The voltammetric behavior of **3** and **4** could be rationalized as an initial one-electron withdrawal from the HOMO of the silatranyl unit (two sequential oxidations of two units in **4**), providing a short-lived cation radical that undergoes structural relaxation to form a pair of N−Si bond length conformers, endo and exo, distributed according to the corresponding activation barriers of their interconversion. Although ET in the endo redox pair seems faster since less internal reorganization is involved, the exo form of the cation radical is a global minimum on the PE curve in solution and the reversibility of ET with endergonic character of electrooxidation of these silatranes provides sufficient driving force to allow the observation of both forms. After the removal of one electron from the 3c-4e bonding scheme (which in fact becomes a much weaker 3c-3e bond, not sufficient to retain the system in endo form), the nitrogen atom in the resulting species adopts the exo configuration which is maintained during fast ET so that the apparent potential of the $\mathbf{3}^{\bullet+}_{exo}/\mathbf{3}_{exo}$ pair (Figures 4 and 5) becomes comparable with the oxidation potential of triethanolamine, in which a N→Si dative interaction is absent. However, the fundamental difference in the oxidation of **3** and **4** and of triethanolamine is that the ET from the former species is reversible while from the latter it is not. Solvation in acetonitrile appears to be an important factor in the electrochemical reactivity of silatranes; therefore, it must be taken into account for correct interpretation of the experiment. A particularly interesting finding is the doubly oxidized form of **4**, which, due to the specific structure of its poorly interacting 3c-4e silatrane systems, might exist as a biradical; it certainly merits a special study.

Reacting oligosilanes **4** with 2 equiv of KO^{t}Bu provides easy access to a 1,4-disilatranyl-1,4-disilanide. Further reaction with 1,2-dichlorotetramethyldisilane led to the formation of a mixture of cis and trans isomers of cyclohexasilane **8**. Interestingly, the silatranyl units in the trans isomer show a substantially diminished Si−N distance and accordingly an elongated Si−SiO_3 distance.

EXPERIMENTAL SECTION

General Remarks. All reactions involving air-sensitive compounds were carried out under an atmosphere of dry nitrogen or argon using either Schlenk techniques or a glovebox. Solvents were dried using a column-based solvent purification system.[52] Compounds **1**,[17] **2**,[17] **3**,[17] **4**,[17] tris(trimethylsilyl)germylpotassium,[25] silatranyl triflate,[17] and 1,2-dichlorotetramethyldisilane[53,54] were prepared according to previously published procedures. All other chemicals were obtained from different suppliers and used without further purification.

^{1}H (300 MHz), ^{13}C (75.4 MHz), and ^{29}Si (59.3 MHz) NMR spectra were recorded on a Varian INOVA 300 spectrometer and are referenced to tetramethylsilane (TMS) for ^{1}H, ^{13}C, and ^{29}Si. In the case of reaction samples a D_2O capillary was used to provide an external lock frequency signal. To compensate for the low isotopic abundance of ^{29}Si, the INEPT pulse sequence[55,56] was used for the amplification of the signal. Elemental analysis was carried out using a Heraeus VARIO ELEMENTAR instrument. For silanides **2a** and **7** elemental analysis was not possible due to their extreme sensitivity. For ***cis*-** and ***trans*-8** elemental analysis did not provide a criterion of purity, since they are isomeric. Therefore, for compounds **2a**, **7**, and ***cis*-** and ***trans*-8** ^{1}H, ^{13}C, and ^{29}Si NMR spectra are provided in the Supporting Information. GC/MS analyses were carried out on an

DOI: 10.1021/acs.organomet.6b00786
Organometallics 2017, 36, 342−351

Agilent 7890A GC instrument (capillary column HP-5MS; 30 m × 0.250 mm; film 0.25 μm) with an Agilent 5975C mass spectrometer.

Voltammetry. Cyclic voltammetry and square wave pulse voltammetry experiments were carried out using a PAR 2373 computer-piloted potentiostat under PAR PowerSuite (release 2.58)[57] software. A conventional 5 mL three-electrode electrochemical cell was used with a Pt-wire counter electrode and an Ag/AgCl reference electrode. The potentials were additionally corrected using E^0 of the reversible couple Fc^+/Fc (0.31 V vs SCE)[58] and brought to the SCE scale for the sake of homogeneity with the previous data. The supporting salt Bu_4NPF_6 (ACROS Organics) was dried over P_2O_5 and activated overnight under vacuum at 80 °C before use. Acetonitrile was distilled from CaH_2 under argon and kept over molecular sieves.

DFT Calculations. DFT calculations of structures and PE profiles of neutral **1** and of its cation radical $\mathbf{1}^{\bullet+}$ along the redundant coordinate *l*(N−Si), including Tomasi's polarized continuum model of acetonitrile solvation (PCM,[59] as implemented in Gaussian 03),[60] were carried out (on HF/6-311G preoptimized structures) using the B3LYP hybrid functional with Lanl2DZ basis set that has been previously shown to provide a good accounting for the experimental features in sila- and germatranes.[12,41] In comparison to PM2, it provides equally chemically sound results at much shorter computation time. The absence of imaginary vibration frequencies was shown at the same level for the structures obtained as global minima.

X-ray Structure Determination. For X-ray structure analyses the crystals were mounted onto the tip of glass fibers, and data collection was performed with a BRUKER-AXS SMART APEX CCD diffractometer using graphite-monochromated Mo Kα radiation (0.71073 Å). The data were reduced to F_o^2 and corrected for absorption effects with SAINT[61] and SADABS,[62] respectively. The structures were solved by direct methods and refined by full-matrix least-squares methods (SHELXL97).[63] If not noted otherwise, all non-hydrogen atoms were refined with anisotropic displacement parameters and all hydrogen atoms were located in calculated positions to correspond to standard bond lengths and angles. Crystallographic data (excluding structure factors) for the structures of compounds **1a**, **2a**, ***cis*-8**, and ***trans*-8** reported in this paper have been deposited with the Cambridge Crystallographic Data Center as supplementary publication nos. CCDC 1477576 (**1a**), 1477575 (**2a**), 1477577 (***cis*-8**), and 1477574 (***trans*-8**); data can be obtained free of charge at http://www.ccdc.cam.ac.uk/products/csd/request/. Figures of solid-state molecular structures were generated using Ortep-3 as implemented in WINGX[64] and rendered using POV-Ray 3.6.[65]

Tris(trimethylsilyl)germylsilatrane (1a). A mixture of tetrakis(trimethylsilyl)germane (1.00 g, 2.74 mmol) and KO^{t}Bu (316 mg, 2.82 mmol) was dissolved in THF (5 mL). The solution turned yellow immediately. After 2 h NMR spectroscopy confirmed the formation of tris(trimethylsilyl)germylpotassium. After THF was removed by putting the sample under vacuum, the germanide was dissolved in toluene (10 mL), whereupon the solution was added dropwise over 1 h to a stirred slurry of silatranyl triflate (973 mg, 3.01 mmol) in toluene (5 mL) at −85 °C. After 12 h toluene was removed under vacuum and the obtained residue was dissolved in pentane and filtered. The colorless solid obtained (870 mg crude yield) was found to be a mixture of tetrakis(trimethylsilyl)germane and tris(trimethylsilyl)-germylsilatrane (**1a**). Due to the thermal sensitivity of **1a**, it was not possible to remove tetrakis(trimethylsilyl)germane by sublimation. Crystallization from pentane yielded **1a** (350 mg, 27%) as colorless crystals. Mp: 170−174 °C. NMR (δ in ppm): ^{1}H ($CDCl_3$) 3.67 (t, *J* = 5.3 Hz, 6H, OCH_2), 2.73 (t, *J* = 5.3 Hz, 6H, NCH_2), 0.19 (s, 27H, $(CH_3)_3Si$); ^{13}C ($CDCl_3$) 58.56 (OCH_2), 52.16 (NCH_2), 2.80 (Me_3Si−Ge); ^{29}Si ($CDCl_3$) −5.6 (Me_3Si), −53.2 (SiO_3). MS (70 eV) *m*/*z* (%): 467(2) [M^+], 452(1) [M^+ − Me], 278(3) [M^+ − $N(CH_2CH_2O)_3Si$ − Me], 219(1) [$(Me_3Si)_2Ge^+$ − H], 174(100) [$N(CH_2CH_2O)_3Si^+$], 73(9) [$SiMe_3^+$]. Anal. Calcd for $C_{15}H_{39}GeNO_3Si_4$: C, 38.62, H, 8.43, N, 3.00. Found: C, 38.99, H, 8.22, N 3.05.

Bis(trimethylsilyl)silatranylgermylpotassium−18-crown-6 (2a). A solution of **1a** (50 mg, 0.107 mmol) KO^{t}Bu (13 mg, 0.112 mmol), and 18-crown-6 (31 mg, 0.112 mmol) in C_6D_6 (1 mL) was left standing for 14 h. After NMR spectroscopic analysis confirmed formation of oligosilatranylgermylpotassium **2a**, the solution mixture was left for crystallization. Pale orange crystals (77 mg, 100%) deposited on the walls of the vial. NMR (δ in ppm): ^{1}H (C_6D_6) 3.81 (t, *J* = 4.9 Hz, 6H, OCH_2), 3.24 (s, 24H, CH_2O), 2.80 (t, *J* = 4.8 Hz, 6H, NCH_2), 0.73 (s, 18H, $(CH_3)_3Si$); ^{13}C (C_6D_6): 70.07 (CH_2O), 60.86 (OCH_2), 54.25 (NCH_2), 7.65 (Me_3Si−Ge); ^{29}Si (C_6D_6) −2.0 (Me_3Si), −13.0 (SiO_3). NMR for ethyl bromide derivatization: ^{1}H (C_6D_6) 3.32 (t, *J* = 5.8 Hz, 6H, OCH_2), 1.82 (t, *J* = 5.8 Hz, 6H, NCH_2), 1.58 (t, *J* = 7.8 Hz, 3H), 1.40 (q, *J* = 7.6 Hz, 2H), 0.53 (s, 18H, $(CH_3)_3Si$); ^{13}C (C_6D_6) 58.28 (OCH_2), 51.20 (NCH_2), 15.03 ($SiCH_2CH_3$), 2.26 ($SiCH_2CH_3$), 1.99 (Me_3Si−Ge); ^{29}Si (C_6D_6) −7.9 (Me_3Si), −58.7 (SiO_3).

2,5-Disilatranyldecamethylhexasilyl-2,5-dipotassium−18-crown-6 (7). A mixture of 2,5-disilatranyl-2,5-bis(trimethylsilyl)-decamethylhexasilane (**4**; 50 mg, 0.061 mmol), KO^{t}Bu (14 mg, 0.129 mmol), and 18-crown-6 (34 mg, 0.129 mmol, 2.05 equiv) was dissolved in C_6D_6 (1 mL) and left for 14 h, after which NMR spectroscopy confirmed quantitative formation of oligosilatranylsilyl-dipotassium (**7**) as a colorless solution. NMR (δ in ppm): ^{1}H (C_6D_6) 3.89 (t, *J* = 5.0 Hz, 12H, OCH_2), 3.31 (s, 48H, CH_2O), 2.87 (t, *J* = 5.1 Hz, 12H, NCH_2), 0.85 (s, 12H, $(CH_3)_2Si$), 0.76 (s, 18H, $(CH_3)_3Si$−Si); ^{13}C (C_6D_6) 70.10 (CH_2O), 60.95 (OCH_2), 54.53 (NCH_2), 7.99 ($(Me_3Si)_2$-Si), 2.76 (Me_2Si); ^{29}Si (C_6D_6) −2.3 ($(Me_3Si)_3Si$), −9.9 (SiO_3), −24.1 (Me_2Si), −209.0 ($(Me_3Si)_3Si$). EI/MS (70 eV) for ethyl bromide derivatization, *m*/*z* (%): 723(1) [M^+ − H], 709(1) [M^+ − Me], 695(1) [M^+ − Et], 651(1) [M^+ − $SiMe_3$], 420(10) [M^+ − $N(CH_2CH_2O)_3SiSi(SiMe_3)Et$], 362(100) [$M^+$ − $N(CH_2CH_2O)_3SiSi(SiMe_3)_2EtSiMe_2$], 174(44) [$N(CH_2CH_2O)_3Si^+$], 73(27) [$SiMe_3^+$].

***cis*-/*trans*-1,4-Disilatranyl-1,4-bis(trimethylsilyl)-octamethylcyclohexasilane (8).** A mixture of 2,5-disilatranyl-2,5-bis(trimethylsilyl)decamethylhexasilane (**4**; 100 mg, 0.123 mmol), KO^{t}Bu (28 mg, 0.253 mmol), and 18-crown-6 (68 mg, 0.253 mmol) was dissolved in benzene (1 mL). After 12 h NMR spectroscopy confirmed formation of **7** and the colorless solution was added dropwise over 15 min to a solution of 1,2-dichlorotetramethyldisilane (25 mg, 0.135 mmol) in toluene (5 mL). After 5 h the volatiles were removed under vacuum and the residue was dissolved in benzene (2 mL) and filtered. A first batch of colorless ***trans*-8** (16 mg, 17%) was obtained by crystallization from benzene. In a second step milky ***cis*-8** (15 mg, 16%) was obtained by crystallization from a 1/2 mixture of acetonitrile and diethyl ether. Data for ***trans*-8** are as follows. Mp: 150−151 °C (decomposition at 302 °C). NMR (δ in ppm): ^{1}H (C_6D_6) 3.33 (t, *J* = 5.6 Hz, 12H, OCH_2), 1.87 (t, *J* = 5.6 Hz, 12H, NCH_2), 0.72 (s, 12H, $(CH_3)_2Si$), 0.71 (s, 12H, $(CH_3)_2Si$), 0.63 (s, 18H, $(CH_3)_3Si$−Si); ^{13}C (C_6D_6) 58.88 (OCH_2), 51.65 (NCH_2), 3.85 ($(Me_3Si)_2$-Si), −1.09 (Me_2Si), −1.26 (Me_2Si); ^{29}Si (C_6D_6) −6.3 ($(Me_3Si)_3Si$), −36.2 (Me_2Si), −52.3 (SiO_3), −130.3 ($(Me_3Si)_3Si$). UV absorption: onset λ 298 nm, shoulder λ 242 nm ($\varepsilon = 2.62 \times 10^4$ M^{-1} cm^{-1}) in THF. Data for ***cis*-8** are as follows. Mp: 198−201 °C. NMR (δ in ppm) ^{1}H (C_6D_6): 3.37 (t, *J* = 5.3 Hz, 12H, OCH_2), 1.89 (t, *J* = 5.3 Hz, 12H, NCH_2), 0.75 (s, 12H, $(CH_3)_2Si$), 0.67 (s, 12H, $(CH_3)_2Si$), 0.59 (s, 18H, $(CH_3)_3Si$−Si); ^{13}C (C_6D_6) 58.95 (OCH_2), 51.88 (NCH_2), 3.67 ($(Me_3Si)_2$-Si), −0.91 (Me_2Si), −1.05 (Me_2Si); ^{29}Si (C_6D_6) −7.8 ($(Me_3Si)_3Si$), −37.5 (Me_2Si), −50.7 (SiO_3), −129.9 ($(Me_3Si)_3Si$). UV absorption: onset λ 303 nm, shoulder λ 242 nm ($\varepsilon = 2.84 \times 10^4$ M^{-1} cm^{-1}) in THF. EI/MS (70 eV) *m*/*z* (%): 782(3) [M^+], 767(1) [M^+ − Me], 709(2) [M^+ − $SiMe_3$], 593(3) [M^+ − $N(CH_2CH_2O)_3SiMe$], 290(5) [$Me_3Si)_3SiMe^+$], 248(3) [$(Me_3Si)_3SiH^+$], 232(7) [[$(Me_3Si)_3SiH^+$ − Me]], 174(100) [$N(CH_2CH_2O)_3Si^+$], 73(21) [$SiMe_3^+$]. Anal. Calcd for $C_{26}H_{66}N_2O_6Si_{10}$: C, 39.85, H, 8.49, N, 3.57. Found: C, 39.44, H, 8.44, N, 3.20.

■ ASSOCIATED CONTENT

Supporting Information

The Supporting Information is available free of charge on the ACS Publications website at DOI: 10.1021/acs.organomet.6b00786.

DOI: 10.1021/acs.organomet.6b00786
Organometallics 2017, 36, 342−351

^{1}H, ^{13}C, and ^{29}Si NMR spectra of compounds **2a**, **7**, ***cis*-8**, and ***trans*-8**, crystallographic data for compounds **1a**, **2a**, ***cis*-8**, and ***trans*-8**, and DFT optimized geometries and Mulliken charges for the calculated structures (PDF)

Cartesian coordinates for calculated structures of **1**, $\mathbf{1}^{\bullet+}_{endo}$, and $\mathbf{1}^{\bullet+}_{exo}$ (XYZ)

Data for all reported crystal structures (CIF)

AUTHOR INFORMATION

Corresponding Authors

*E-mail for J.B.: baumgartner@tugraz.at.

*E-mail for V.V.J.: viatcheslav.jouikov@univ-rennes1.fr.

*E-mail for C.M.: christoph.marschner@tugraz.at.

ORCID

Christoph Marschner: 0000-0001-8586-2889

Notes

The authors declare no competing financial interest.

ACKNOWLEDGMENTS

Support for this study was provided by the Austrian *Fonds zur Förderung der wissenschaftlichen Forschung* (FWF) via the projects P-26417 (C.M.) and P-25124 (J.B.).

REFERENCES

(1) Puri, J. K.; Singh, R.; Chahal, V. K. *Chem. Soc. Rev.* **2011**, *40*, 1791−1840.

(2) Pestunovich, V.; Kirpichenko, S.; Voronkov, M. In *The Chemistry of Organic Silicon Compounds*; Rappoport, Z., Apeloig, Y., Eds.; Wiley: Chichester, U.K., 2003; pp 1447−1537.

(3) Verkade, J. G. *Coord. Chem. Rev.* **1994**, *137*, 233−295.

(4) Voronkov, M. G.; Dyakov, V. M.; Kirpichenko, S. V. *J. Organomet. Chem.* **1982**, *233*, 1−147.

(5) Voronkov, M. G. *Pure Appl. Chem.* **1966**, *13*, 35−59.

(6) Gordon, M. S.; Carroll, M. T.; Jensen, J. H.; Davis, L. P.; Burggraf, L. W.; Guidry, R. M. *Organometallics* **1991**, *10*, 2657−2660.

(7) Schmidt, M. W.; Windus, T. L.; Gordon, M. S. *J. Am. Chem. Soc.* **1995**, *117*, 7480−7486.

(8) Trofimov, A. B.; Zakrzewski, V. G.; Dolgounitcheva, O.; Ortiz, J. V.; Sidorkin, V. F.; Belogolova, E. F.; Belogolov, M.; Pestunovich, V. A. *J. Am. Chem. Soc.* **2005**, *127*, 986−995.

(9) Savéant, J.-M.; Tidwell, T. T. *Adv. Phys. Org. Chem.* **2000**, *35*, 117−192.

(10) Broka, K.; Glezer, V.; Stradiņš, J.; Zelčans, G. *Zh. Obshch. Khim.* **1991**, *61*, 1374−1378.

(11) Broka, K.; Stradiņš, J.; Glezer, V.; Zelcans, G.; Lukevics, E. *J. Electroanal. Chem.* **1993**, *351*, 199−206.

(12) Jouikov, V. *ECS Trans.* **2010**, *28*, 5−16.

(13) Ignatovich, L.; Jouikov, V. *J. Organomet. Chem.* **2014**, *751*, 546−554.

(14) Singh, G.; Saroa, A.; Garg, M.; Sharma, R. P.; Gubanov, A. I.; Smolentsev, A. I. *J. Organomet. Chem.* **2012**, *719*, 21−25.

(15) Zaitsev, K. V.; Churakov, A.; Poleshchuk, O. K.; Oprunenko, Y. F.; Zaitseva, G. S.; Karlov, S. S. *Dalton Trans.* **2014**, *43*, 6605−6609.

(16) Yamamoto, Y.; Matsubara, H.; Murakami, K.; Yorimitsu, H.; Osuka, A. *Chem. - Asian J.* **2015**, *10*, 219−224.

(17) Aghazadeh Meshgi, M.; Baumgartner, J.; Marschner, C. *Organometallics* **2015**, *34*, 3721−3731.

(18) Wallner, A.; Emanuelsson, R.; Baumgartner, J.; Marschner, C.; Ottosson, H. *Organometallics* **2013**, *32*, 396−405.

(19) Wallner, A.; Hlina, J.; Wagner, H.; Baumgartner, J.; Marschner, C. *Organometallics* **2011**, *30*, 3930−3938.

(20) Wallner, A.; Hlina, J.; Konopa, T.; Wagner, H.; Baumgartner, J.; Marschner, C.; Flörke, U. *Organometallics* **2010**, *29*, 2660−2675.

(21) Wallner, A.; Wagner, H.; Baumgartner, J.; Marschner, C.; Rohm, H. W.; Kockerling, M.; Krempner, C. *Organometallics* **2008**, *27*, 5221−5229.

(22) Marschner, C.; Baumgartner, J.; Wallner, A. *Dalton Trans.* **2006**, 5667−5674.

(23) Hlina, J.; Stella, F.; Aghazadeh Meshgi, M.; Marschner, C.; Baumgartner, J. *Molecules* **2016**, *21*, 1079.

(24) Marschner, C. *Eur. J. Inorg. Chem.* **1998**, *1998*, 221−226.

(25) Fischer, J.; Baumgartner, J.; Marschner, C. *Organometallics* **2005**, *24*, 1263−1268.

(26) Derouiche, Y.; Lickiss, P. D. *J. Organomet. Chem.* **1991**, *407*, 41−49.

(27) Meshgi, M. A. Ph.D. thesis, Technische Universität Graz, Graz, Austria, 2015.

(28) Whittaker, S. M.; Brun, M.-C.; Cervantes-Lee, F.; Pannell, K. H. *J. Organomet. Chem.* **1995**, *499*, 247−252.

(29) Kayser, C.; Kickelbick, G.; Marschner, C. *Angew. Chem., Int. Ed.* **2002**, *41*, 989−992.

(30) Miller, R. D.; Michl, J. *Chem. Rev.* **1989**, *89*, 1359−1410.

(31) Diaz, A.; Miller, R. D. *J. Electrochem. Soc.* **1985**, *132*, 834−837.

(32) Boberski, W. G.; Allred, A. L. *J. Organomet. Chem.* **1975**, *88*, 65−72.

(33) Voronkov, M. G.; Brodskaya, E. I.; Belyaeva, V. V.; Kashik, T. V.; Baryshok, V. P.; Yarosh, O. G. *Zh. Obshch. Khim.* **1986**, *56*, 621−627.

(34) Malachesky, P. A. *Anal. Chem.* **1969**, *41*, 1493−1494.

(35) Zhuikov, V. *Russ. J. Gen. Chem.* **1999**, *69*, 1906−1911.

(36) Zhuikov, V. *Russ. J. Gen. Chem.* **1999**, *70*, 879−884.

(37) Mochida, K.; Itani, A.; Yokoyama, M.; Tsuchiya, T.; Worley, S. D.; Kochi, J. K. *Bull. Chem. Soc. Jpn.* **1985**, *58*, 2149−2150.

(38) Fukuzumi, S.; Kitano, T.; Mochida, K. *Chem. Lett.* **1990**, *19*, 1741−1744.

(39) Watanabe, H.; Yoshizumi, K.; Muraoka, T.; Kato, M.; Nagai, Y.; Sato, T. *Chem. Lett.* **1985**, *14*, 1683−1686.

(40) Cleij, T. J.; King, J. K.; Jenneskens, L. W. *Chem. Mater.* **2000**, *12*, 84−89.

(41) Imae, I.; Minami, T.; Kawakami, Y. *Des. Monomers Polym.* **2004**, *7*, 127−133.

(42) Cerveau, G.; Chuit, C.; Colomer, E.; Corriu, R. J. P.; Reye, C. *Organometallics* **1990**, *9*, 2415−2417.

(43) Marcus, R. A. In *Special Topics in Electrochemistry*; Rock, P. A., Ed.; Elsevier: Amsterdam, 1977; pp 161−170.

(44) Soualmi, S.; Dieng, M.; Ourari, A.; Gningue-Sall, D.; Jouikov, V. *Electrochim. Acta* **2015**, *158*, 457−469.

(45) Amatore, C. In *Organic Electrochemistry*, 4th ed.; Hammerich, O., Lund, H., Eds.; CRC Press: Boca Raton, FL, 2000.

(46) Isaacs, N. S. In *Physical Organic Chemistry*; The University Press: Belfast, Northern Ireland, 1987; p 828.

(47) Hammerich, O. In *Organic Electrochemistry*, 4th ed.; Hammerich, O., Lund, H., Eds.; CRC Press: Boca Raton, FL, 2000; p 102.

(48) Fischer, R.; Frank, D.; Gaderbauer, W.; Kayser, C.; Mechtler, C.; Baumgartner, J.; Marschner, C. *Organometallics* **2003**, *22*, 3723−3731.

(49) Fischer, R.; Konopa, T.; Ully, S.; Baumgartner, J.; Marschner, C. *J. Organomet. Chem.* **2003**, *685*, 79−92.

(50) Fischer, R.; Konopa, T.; Ully, S.; Wallner, A.; Baumgartner, J.; Marschner, C. In *Organosilicon Chemistry VI*; Auner, N., Weis, J., Eds.; Wiley-VCH: Weinheim, Germany, 2005; pp 355−360.

(51) West, R. *Pure Appl. Chem.* **1982**, *54*, 1041−1050.

(52) Pangborn, A. B.; Giardello, M. A.; Grubbs, R. H.; Rosen, R. K.; Timmers, F. J. *Organometallics* **1996**, *15*, 1518−1520.

(53) Ishikawa, M.; Kumada, M.; Sakurai, H. *J. Organomet. Chem.* **1970**, *23*, 63−69.

(54) Marschner, C.; Baumgartner, J. In *Science of Synthesis: Houben-Weyl Methods of Molecular Transformations*; Oestreich, M., Ed.; Thieme: Stuttgart, Germany, 2013.

(55) Morris, G. A.; Freeman, R. *J. Am. Chem. Soc.* **1979**, *101*, 760−762.

(56) Helmer, B. J.; West, R. *Organometallics* **1982**, *1*, 877−879.

DOI: 10.1021/acs.organomet.6b00786
Organometallics 2017, 36, 342−351

(57) *PAR PowerSuite 2.58, I/O Library 2.43.0*; Princeton Applied Research, Princeton, NJ, 2003.
(58) Mann, C. K.; Barnes, K. K. *Electrochemical Reactions In Nonaqueous Systems*; Marcel Dekker: New York, 1970.
(59) Tomasi, J.; Mennucci, B.; Cammi, R. *Chem. Rev.* **2005**, *105*, 2999−3094.
(60) Frisch, M. J.; Trucks, G. W.; Schlegel, H. B.; Scuseria, G. E.; Robb, M. A.; Cheeseman, J. R.; Montgomery, J. A., Jr.; Vreven, T.; Kudin, K. N.; Burant, J. C.; Millam, J. M.; Iyengar, S. S.; Tomasi, J.; Barone, V.; Mennucci, B.; Cossi, M.; Scalmani, G.; Rega, N.; Petersson, G. A.; Nakatsuji, H.; Hada, M.; Ehara, M.; Toyota, K.; Fukuda, R.; Hasegawa, J.; Ishida, M.; Nakajima, T.; Honda, Y.; Kitao, O.; Nakai, H.; Klene, M.; Li, X.; Knox, J. E.; Hratchian, H. P.; Cross, J. B.; Bakken, V.; Adamo, C.; Jaramillo, J.; Gomperts, R.; Stratmann, R. E.; Yazyev, O.; Austin, A. J.; Cammi, R.; Pomelli, C.; Ochterski, J. W.; Ayala, P. Y.; Morokuma, K.; Voth, G. A.; Salvador, P.; Dannenberg, J. J.; Zakrzewski, V. G.; Daniels, A. D.; Strain, M. C.; Farkas, O.; Malick, D. K.; Rabuck, A. D.; Raghavachari, K.; Foresman, J. B.; Ortiz, J. V.; Cui, Q.; Baboul, A. G.; Clifford, S.; Cioslowski, J.; Stefanov, B. B.; Liu, G.; Liashenko, A.; Piskorz, P.; Komaromi, I.; Fox, D. J.; Al-Laham, M. A.; Peng, C. Y.; Nanayakkara, A.; Challacombe, M.; Gill, P. M. W.; Johnson, B.; Chen, W.; Wong, M. W.; Gonzalez, C. C.; Pople, J. A. *Gaussian 03, Revision D.01*; Gaussian, Inc., Wallingford, CT, 2004.
(61) *SAINTPLUS: Software Reference Manual, Version 6.45*; Bruker-AXS: Madison, WI, 1997−2003.
(62) Sheldrick, G. M. *SADABS, Version 2.10*; Bruker AXS Inc., Madison, WI, 2003.
(63) Sheldrick, G. M. *Acta Crystallogr., Sect. A: Found. Crystallogr.* **2008**, *64*, 112−122.
(64) Farrugia, L. J. *J. Appl. Crystallogr.* **2012**, *45*, 849−854.
(65) *POVRAY 3.6*; Persistence of Vision Pty. Ltd., Williamstown, Victoria, Australia, 2004; available online at http://www.povray.org/download/ (accessed on 09.07.2008).

DOI: 10.1021/acs.organomet.6b00786
Organometallics 2017, 36, 342−351